Correlative Analysis of Hard and Soft X-ray Emissions in Solar Flares

FINAL REPORT

S-57783-F

Submitted to:

NASA/GSFC Greenbelt, MD 20771

Submitted by:

Dominic M. Zarro
Applied Research Corporation,
8201 Corporate Dr. Landover, MD 20785.

Date:

May 20, 1997

1. INTRODUCTION

This report describes research performed under the Phase 5 *Compton Gamma-Ray Observatory (CGRO)* Guest Investigator Program. The objective of this work is to study different mechanisms of solar flare heating by comparing their predictions with simultaneous hard and soft X-ray observations. The datasets used in this work consist of hard X-ray observations from the *CGRO* Burst and Transient Source Experiment (BATSE) and soft X-ray observations from the Bragg Crystal Spectrometer (BCS) and Soft X-ray telescope (SXT) on the Japanese *Yohkoh* spacecraft.

2. WORK PERFORMED

Research focussed on developing methods for determining the thermodynamic conditions in solar flares in which DC-electric field acceleration is responsible for producing impulsive non-thermal hard X-ray emission. The plasma temperature and density are two critical parameters that affect the efficiency of runaway acceleration. In particular, under low density and high temperature conditions, electron runaway acceleration is expected to dominate as a greater fraction of thermal electrons have sufficiently large velocities to undergo runaway. With increasing density, such as would occur during chromospheric evaporation, collisional redistribution inhibits the runaway process by thermalizing these high velocity electrons. Hence, inorder to overcome this density "quenching" effect and sustain the production of nonthermal electrons by runaway acceleration, the electron temperature within the acceleration region must increase significantly during the flare. The following analysis presents a method for deducing the temperature in the acceleration region by combining simultaneous *Yohkoh* soft X-ray and *CGRO* BATSE hard X-ray obseravations, and comparing the results with measurements of "super-hot" temperatures in solar flares.

DC-electric fields and their associated electric currents have been shown to provide a viable mechanism for heating plasma and accelerating electrons in solar flares (Tsuneta 1985, Holman 1985). We deduce the temperature in the acceleration region by solving the energy balance equation in a 1-dimensional loop consisting of field-aligned currents. The energy balance equation is expressed as,

$$dU/dt = Q - R - dF_c/dz - 5nkTdv/dz, \tag{1}$$

where $U = 3nkT$ is the thermal energy per unit volume, Q is the total flare heating rate, $F_c \simeq -10^{-6}T^{5/2}dT/dz$ is the Spitzer conductive heat flux, $R \simeq an^2T^{-1/2}$ is the optically thin cooling rate, and the velocity gradient term is the enthalpy flux of evaporative motions within the loop.

We model the loop as a two-component plasma consisting of current-heated flux tubes with total volume V_f (in which electrons are runaway-acclerated), and a surrounding volume V_s which is not directly heated by currents but is in thermal and pressure equlibrium with the current-heated plasma. Such "filamentation" of the loop plasma is expected from electrodynamic arguments. In

particular, for a loop current system to remain stable, the total induction magnetic field strength of current-carrying electrons (drifting and accelerated electrons) must be less than that of the ambient coronal magnetic field (Holman 1985).

We represent the temperature and density within each filament by T_f and n_f, and the corresponding values in the surrounding plasma by T_s and n_s, respectively. The density and temperature within the filamented and surrounding regions are assumed to be uniform along the loop length. This approximation is expected to become valid approximately 20–30 s after heating onset when conduction will have redistributed the heat energy throughout the loop, and hydrodynamic motions will have restored approximate pressure balance within the loop (Fisher 1989). Accordingly, we simplify equation (1) by spatially averaging it with respect to the total loop volume $V(= V_f + V_s)$ such that,

$$\dot{U}_f V_f + \dot{U}_s V_s = Q_f V_f - R_f V_f - R_s V_s \qquad (2),$$

where Q_f is the heating rate within the filaments. The enthalpy and conductive terms vanish at the loop apex and are negligible in the chromosphere ($z = 0$) relative to the heating and cooling terms. From pressure-balance, $T_f n_f = T_s n_s$ which implies $U_s = U_f$ and which further reduces the energy balance equation to,

$$\dot{U}_s V = Q_f V_f - R_f V_f - R_s (V - V_f) \qquad (3).$$

The filament heating rate consists of a Joule heating term given by,

$$Q_{curr} = n_f k T_f \nu_e (E/E_D)^2 \qquad \text{ergs cm}^{-3}\ \text{s}^{-1} \qquad (4)$$

where $\nu_e \approx 3.2 \times 10^2 n_f {T_f}^{-3/2}$ s^{-1} is the thermal collision frequency (for classical resistivity), E is the electric field strength (assumed uniform along the loop length), and $E_D = 7 \times 10^{-8} n_f {T_f}^{-1}$ volts cm^{-1} is the Dreicer field (Dreicer 1959). The Dreicer field is the field strength at which all the electrons in the current filaments plasma undergo thermal runaway. The heating rate also contains a Coulomb heating term due to accelerated electrons that propagate along the flare loop. For a power-law spectrum of electrons, the loop-integrated collisional heating rate assuming thick-target electrons is approximated by (Lin and Hudson 1976),

$$Q_{elec} = 1.6 \times 10^{-9} \gamma (\gamma - 1)^{-1} E_c \dot{N} \qquad \text{ergs s}^{-1} \qquad (5),$$

where,

$$\dot{N}_{thick} \simeq 3 \times 10^{33} a_1 (\gamma - 1)^2 B(\gamma - 1/2, 1/2) {E_c}^{-\gamma} \qquad \text{s}^{-1} \qquad (6),$$

is the total number flux of nonthermal electrons, a_1 and $\gamma = \delta - 1$ are the amplitude and spectral index, respectively, for a power-law approximation to the nonthermal hard X-ray spectrum

produced by the electrons, and E_c is the low-energy cutoff of the electron energy spectrum. For electrons produced by runaway acceleration the number flux is given by,

$$\dot{N}_{run} \simeq .35 n_c \nu_e (E_D/E)^{3/8} \exp[-2^{1/2}(\mathrm{E_D/E})^{1/2} - (1/4)(\mathrm{E_D/E})]\mathrm{V_f} \qquad \mathrm{s}^{-1} \qquad (7),$$

which includes electrons that are accelerated out of the thermal distribution as well as electrons that are scattered into the runaway regime by collisions (Holman 1985).

Substituting the above heating terms into the energy balance equation we obtain,

$$\dot{U}_s V = Q_{curr} V_f + Q_{elec} - R_f V_f - R_s (V - V_f) \qquad (8).$$

The energy balance equation consists of 4 unknowns: T_f, n_f, V_f, and E. We eliminate n_f by using pressure balance to relate the temperature and density within individual current filaments to the corresponding values in the larger surrounding loop volume such that $n_f = T_s n_s / T_f$. We eliminate V_f by equating the thick-target electron flux (eq. 6) with the theoretical electron runaway flux (eq. 7). The energy balance equation is thus reduced to the two unknowns T_f and E and the quantities V, T_s, and n_s which are constrained by observations. In particular, we equate the total loop volume with the observed loop volume $V = 2AL$, where A is the observed loop area and L is the loop half-length. We infer T_s from soft X-ray observations of the thermal plasma using the temperature-sensitive Ca XIX resonance line (§ 3), and n_s from the Ca XIX emission measure $EM \approx n_s^2 V_s$.

3. RESULTS

The energy balance equation could not be solved uniquely for E and T_f without an additional constraining relation between these two parameters. One approach is to exploit the relationship between the critical energy for runaway acceleration and the electron low-energy cutoff E_c. The critical energy separates thermal and runaway electrons and is given by $E_{crit} = m_e {v_f}^2/2$ where v_f is the threshold velocity above which thermal electrons exceed frictional forces and runaway (Benka 1991, Benka and Holman 1992). This threshold velocity is given by $v_f = (E_D/E)^{1/2} v_e$ where $v_e = 2kT_f/{m_e}^{1/2}$ is the electron thermal velocity. Setting $E_c = E_{crit}$, we derive $E/E_D = E_c/(2kT_f)$. Substituting the latter into equation (8), we can solve for T_f for different specified values of E_c that are assumed constant during the flare. In this manner, we produce a grid of (T_f, E_c) solutions as a function of time during the flare.

We applied this technique to three flares that were observed simultaneously by *CGRO* BATSE and *Yohkoh* BCS and SXT. The first flare was an M1.9 event that occurred at 15:40 UT on 1992 February 17 (Kucera *et al.* 1996). The second was an M3.3 event that occurred at 09:00 UT on 1992 September 6 (Zarro, Mariska, and Dennis 1995). The third event was the famous impulsive loop-top flare that occurred at 17:27 UT on 1992 January 13 (Masuda 1993). For each flare we used SXT Beryllium filter images obtained at the onset of the hard X-ray impulsive phase to determine the characteristic soft X-ray loop volume. We determined the electron temperature

and plasma emission measure from least-squares fits of synthetic spectra to the Ca XIX resonance and dielectronic lines observed with the BCS. Figure 1 shows a sample fitted Ca XIX spectrum for the September flare.

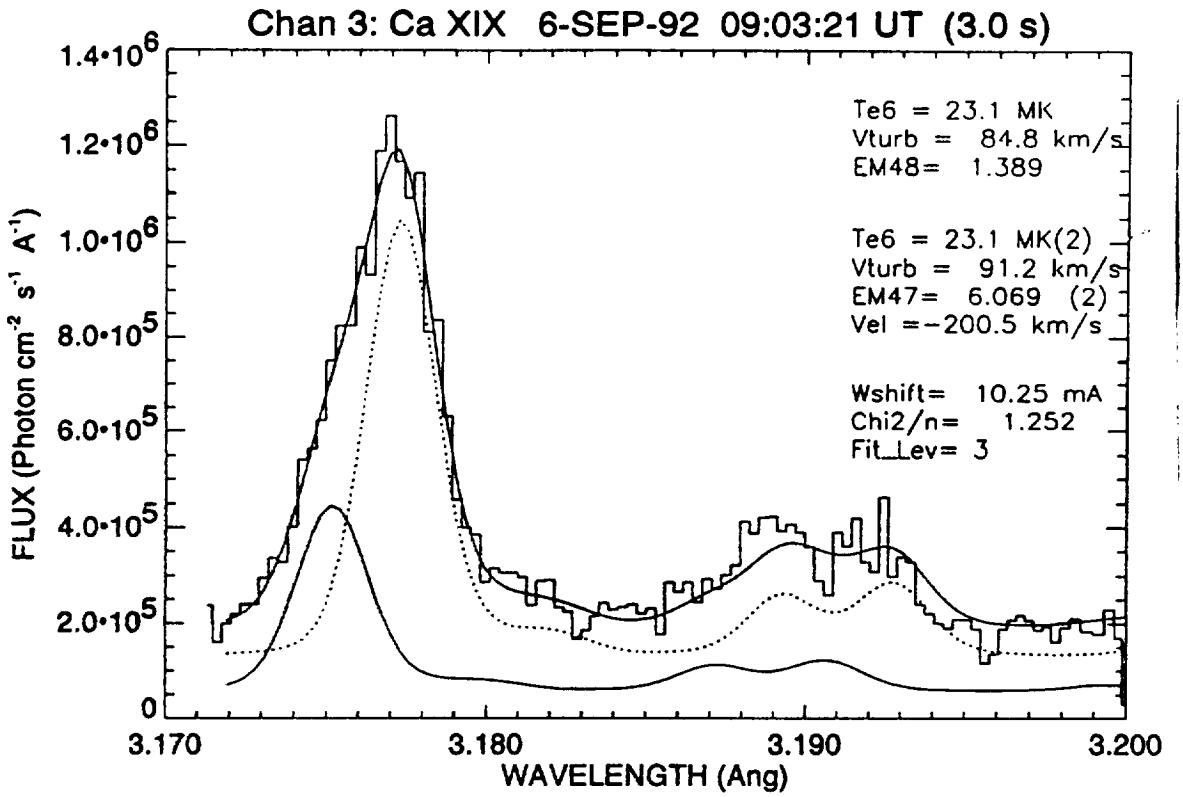

Figure 1. A two-component fit to the *Yohkoh*/BCS Ca XIX spectrum for the 1992 September 6 flare. The fit yields the temperature, emission measure (hence, density), and velocity upflow for the flare thermal component.

We used the BATSE LAD Continuous data to derive the nonthermal hard X-ray parameters of each flare. This data type produces hard X-ray spectra in 16 channels between 10 and > 1000 keV at 2.048 sec temporal resolution. We modelled the deconvolved LAD spectra in the 20-100 keV range with a power-law function of the form $I = a_1 \epsilon^{-\gamma}$ and used a least-squares fitting technique to infer a_1 and γ. Figure 2 shows a sample fitted power-law spectrum for one of the LAD flare intervals.

We developed Interactive Data Language (IDL) code to iteratively solve equation (8) for times when overlapping BCS and BATSE data were available. Generally, the signal-to-noise in both datasets was optimum during the main hard X-ray emission phase. Hard and soft X-ray fluxes were typically too weak during the early rise phase to produce reliable spectral fits. During

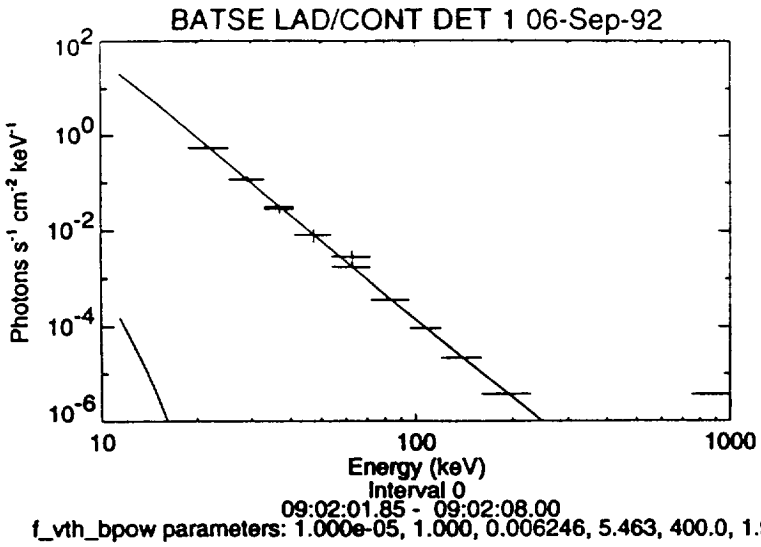

Figure 2. Power-law fit to the BATSE LAD CONT spectrum at the time of the first hard X-ray burst for the flare observed on 1992 September 6

this initial rapid heating phase, the assumptions of uniform temperature and density are not applicable. We created a grid of constant low-energy cutoff models ranging between $E_c = 10$ and 50 keV, in steps of 5 keV. For each E_c, we solved equation (8) for the variation of T_f using the empirical values of a_1, γ, T_s, n_s, and V.

For all three events, we found that no solutions could be obtained for values of E_c below 30 keV. For these "low" cutoff energies, the implied number flux of nonthermal thick-target electrons (eq. 6), exceeded the predicted flux of runaway electrons (eq. 7) by orders of magnitude. For $E_c > 30$ keV, several temperature solutions were found that yielded agreement between observed and predicted electron fluxes. Figure 3 illustrates these solutions for the 13 January and 17 February flares for selected values of E_c. The computed loop filament temperatures are compared with the Ca XIX-soft X-ray temperatures, and with simultaneous measurements of the "super-hot" temperature component derived from fits of a thermal bremsstrahlung model to low-energy (< 20 keV) hard X-ray emission. In each flare, the Ca XIX-inferred temperatures (which are associated with the non-current heated loop region) were considerably cooler than T_f. In the case of the 13 January flare, the super-hot temperature was derived from the BATSE high resolution spectroscopy detector (SD) which consists of 256 channels. Figure 4 shows a sample fit of a bremsstrahlung plus power-law component to one of the SD flare intervals. The super-hot temperatures varied in the range $33-38\times10^6$ K, which matched closely the filament temperature variation corresponding to $E_c = 35$ keV. For the 17 February event, the super-hot temperature was derived by Kucera *et al.* (1996) using the L (15-24 keV) and M1 (24-35 keV) channel ratios of the *Yohkoh* Hard X-ray Telescope. Although the super-hot temperature correlated closely with the overall variation of T_f, it could not be a matched by a single value of E_c, but instead with

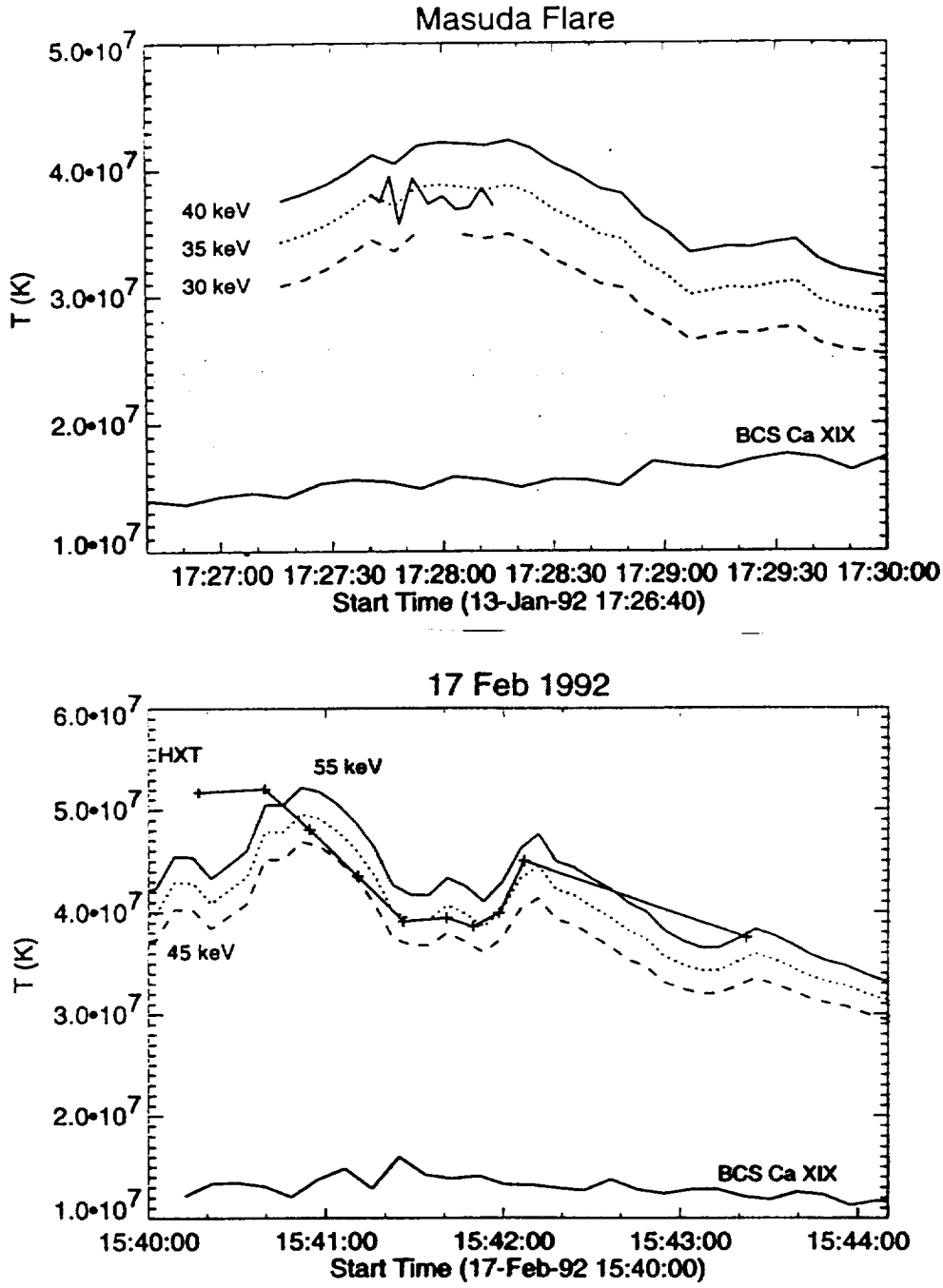

Figure 3. Loop filament temperatures T_f (smooth labelled curves) computed for different electron low-energy cutoff E_c values in the 13 January (upper panel) and 17 February (lower panel) flares. Shown for comparison are the cooler Ca XIX-inferred temperatures which are associated with the non-current heated loop plasma, and the "super-hot" HXR-inferred temperatures which are associated with the current heated regions.

values of E_c in the range 45–55 keV.

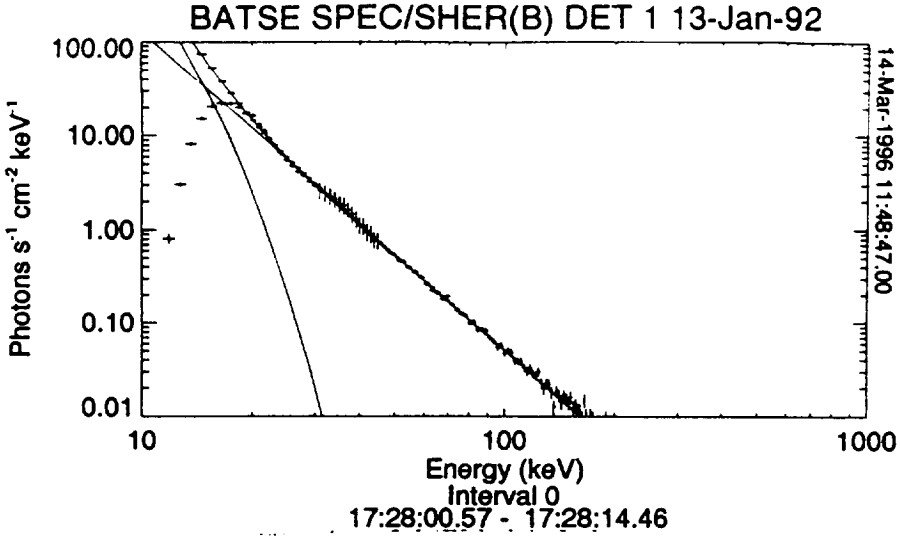

Figure 4. Thermal bremsstrahlung plus power-law fit to the BATSE Spectral Detector SHERB spectrum at the time of the first hard X-ray burst for the flare observed on 1992 January 13

4. SUMMARY

The main conclusion of our work is that the DC-electric field heating and acceleration model can explain the thermal and nonthermal properties of solar flares in a manner consistent with energy balance. Inorder for the model to self-consistently explain thermal soft X-ray emission and nonthermal hard X-ray emission, our simple energy balance calculations indicate that a "super-hot" component must exist within the flaring loop. This "super-hot" component is necessary to ensure a sufficient supply of thermal electrons to offset the collisional thermalization that occurs when the density within the loop increases because of chromospheric evaporation. The "super-hot" region is associated with a current-heated region that is cospatial with the electron runaway-acceleration region. In our analysis, the "super-hot" component arises in filamentary structures that extend along the length of a coronal loop in which Joule current-heating and runaway electron acceleration occur simultaneously. The observation of hard X-rays in footpoints with opposite magnetic polarity, suggest that a fraction (50 %) of the total number of filaments must have electric field components that are directed in opposite directions.

REFERENCES

Benka, S.G. 1991, Ph.D. Thesis, Univ. of North Carolina, Chapel Hill

Benka, S.G., and Holman, G.D. 1992, ApJ, 391, 854

Dreicer, H. 1959, Phys. Rev., 115, 238

Fisher, G.F. 1989, ApJ, 346, 1019

Holman, G.D. 1985, ApJ, 293, 584

Holman, G.D., Kundu, M., and Kane, S. 1989, ApJ, 345, 1050

Kucera, T.A., Love, P.J., Dennis, B.R., Holman, G.D., Schwartz, R.A., and Zarro, D.M. 1996, ApJ, 466, 1067

Lin, R.P.. and Hudson, H.S. 1976, Solar Phys., 50, 153

Masuda, S. 1993, PhD Thesis, University of Tokyo

Tsuneta, S. 1985, ApJ, 290, 353

Zarro, D.M., Mariska, J.T., and Dennis, B.R. 1995, ApJ, 440, 888

NASA

Report Documentation Page

1. Report No.	2. Government Accession No.	3. Recipient's Catalog No.

4. Title and Subtitle
"Correlative Analysis of Hard and Soft X-ray in Solar Flares"

5. Report Date
May 20, 1997

6. Performing Organization Code

7. Author(s)
Dr. Dominic Zarro

8. Performing Organization Report No.
R97-257

10. Work Unit No.

9. Performing Organization Name and Address
Applied Research Corporation
8201 Corporate Drive
Suite 1120
Landover, MD 20785

11. Contract or Grant No.
S-57783-F

13. Type of Report and Period Covered
Final Report 11/02/95 thru 05/01/97.

12. Sponsoring Agency Name and Address
NASA/Goddard Space Flight Center
Greenbelt, MD 20771

14. Sponsoring Agency Code

15. Supplementary Notes

16. Abstract

We propose to continue a study that we have commenced under the Cycle 3 and 4 GI programs. Our broad aim is to test flare models by comparing their predictions with simultaneous BATSE hard X-ray and Yohkoh soft X-ray observations. For Cycle 5, we will focus on the hydrodynamic consequences of current heating and runaway acceleration. We will use BATSE spectra in the 20-300 keV range from the Large Area detectors to deduce the nonthermal hard X-ray component that is related to the electron heating rate. We will use Yohkoh soft X-ray data to deduce the thermal heating rate and the plasma cooling rates of the evaporating chromospheric component. By comparing these rates, we will place tighter constraints on the physical parameters that control heating and acceleration in solar flares.

17. Key Words (Suggested by Author(s))	18. Distribution Statement		
Sun, Flares, Corona			
19. Security Classif. (of this report)	20. Security Classif. (of this page)	21. No. of pages	22. Price